Invited Speaker

1189 Pushing the limits of Coupled Extreme Environments during In-situ TEM
Professor Khalid Hattar

Oral Presentation

105 Localized, anodic aluminum corrosion phenomena studied with electrochemical liquid phase electron microscopy
Morgan Binggeli Barbey[1], Prof. Vasiliki Tileli[1]
[1]Ecole polytechnique fédérale de Lausanne (EPFL), Lausanne, Switzerland
218 Deformation mechanisms of inorganic fullerenes used as lubrication additives: an in situ TEM nanocompression study
Dr Sankar RK Pattamadai Sundaram[1], Dr Lucile Joly-Pottuz[1], Dr Pavel Afanasiev[2], Miss Marina Benmansour[3], Pr Fabrice Dassenoy[3], Pr Karine Masenelli-Varlot[1]
[1]MATEIS - INSA Lyon, Villeurbanne, France, [2]IRCELYON - UCBL, Villeurbanne, France, [3]LTDS - ECL, Ecully, France
497 In-situ nucleation of silicon particles using environmental transmission electron microscopy
Dr Lucian Roiban[1], Dr. Cynthia Cibaka-Ndaya[2], Dr. Kevin O'Connor[3], M. Emmanuel Opeyemi Idowu[2], Professor Jonhatan G.-C. Veinot[3], Dr. Glenna L. Drisko[2]
[1]INSA Lyon, Université Claude Bernard Lyon 1, CNRS, MATEIS, UMR5510, Villeurbanne, France, [2]ICMCB, UMR 5026, CNRS, Univ. Bordeaux, Bordeaux INP, Pessac F-33600, France, [3]Department of Chemistry, The University of Alberta, Edmonton, Canada
522 Study of nuclear materials for silicon carbide composite fuel claddings via STEM, EDX and EELS
Phd Student Hector Guerra Yanez[1], PhD Student Andrea Stinchelli[2,3], Doctor Fabio Di Fonzo[3], Professor Per O.Å. Persson[1]
[1]Department of Physics, Chemistry and Biology, University of Linköping, Linköping, Sweden, [2]Department of Energy, Politecnico di Milano, Milan, Italy, [3]X-nano s.r.l., Milan, Italy
763 In-situ TEM ion irradiation studies of layered MAX phase materials
Mrs Eman Al Ruqeishi[1], Max Rigby-Bell[2], Graeme Greaves[3], Alexander Eggeman[1], Sarah Haigh[1]
[1]University of Manchester, Manchester, United Kingdom, [2]UK Atomic Energy Authority, Abingdon, United Kingdom, [3]University of Huddersfield, Huddersfield, United Kingdom
1029 Correlative microscopy of creep cavitation in steels using image processing of SEM, FIB-XeF2 and EBSD
Dr Tomas Martin[1], Dr Siqi He[1], Ms Eirini Gallioupolou[1], Mr Peter Thomas[1], Mr Edward Horton[1], Mr Michael Salvini[1], Dr Nicolo Grilli[1], Professor David Knowles[1], Professor Mahmoud Mostafavi[1], Professor Peter Flewitt[1]
[1]University of Bristol, Bristol, United Kingdom

Poster Presentation

300 In situ scanning precession electron diffraction study of chemo-mechanical interactions during Zr oxidation
Dr. Dan Zhou[2,3], Yongwen Sun[1], Dr. Ying Han[1], Dr. H. Hugo Perez Garza[3], Dr. Alejandro Gomez Perez[4], Dr. Athanassios S. Galanis[4], Dr. Stavros Nicolopoulos[4], Prof. Dr. Yang Yang[1]
[1]Department of Engineering Science and Mechanics and Materials Research Institute, The Pennsylvania State University, University Park, PA, 16802, United States, [2]Leibniz Institute for Crystal Growth, Berlin, 12489, Germany, [3]DENSsolutions B.V., Delft, 2628 ZD, Netherlands, [4]NanoMegas SPRL, Brussels, 1050, Belgium
643 In- and ex-situ implantation of helium to characterise faults in titanium beryllide

Dr Jo Sharp[1], Dr Slava Kuksenko[2], Dr Ramil Gaisin[3], Professor Jonathan Hinks[1], Dr Graeme Greaves[1], Professor Stephen Donnelly[1], Professor Pavel Vladimirov[3]
[1]University of Huddersfield, Huddersfield, United Kingdom, [2]UKAEA, Culham, United Kingdom, [3]Karlsruhe Institute of Technology, Karlsruhe, Germany

1041 Using XeF2 FIB imaging to contrast and quantify precipitation in metal.

Mr Peter Thomas[1], Dr Mariia Zimina[1], Dr Lawrence Coghlan[1], Mr Aidan Gunn[1], Dr Siqi He[1], Dr Aya Shin[2], Dr Jonathan Pearson[2], Professor Peter Flewitt[1], Dr Tomas Martin[1]
[1]University of Bristol, Bristol, United Kingdom, [2]EDF UK, Gloucester, United Kingdom

1073 Influence of damage dose on the defect formation in tungsten

Dipl.-Ing. Ute Jäntsch[1], Dr. Michael Klimenkov[1], Dr. Michael Rieth[1], Dr. Thomas Schwarz-Selinger[2], Dr. Mikhail Zibrov[2]
[1]Institute of Applied Materials, Karlsruhe Institute of Technology, Eggenstein-Leopoldshafen, Germany, [2]Max-Planck-Institut für Plasmaphysik (IPP), Garching, Germany

1077 Corrosion of Alloys Suitable for Very High Temperature Systems (VHTRs) Exposed to High Temperature Helium

Dr Lawrence Coghlan[1], Dr Mariia Zimina[1], Dr Robert Burrows[3], Dr Aya Shin[2], Dr Tomas Martin[1]
[1]University of Bristol, Bristol, United Kingdom, [2]EDF Energy, Gloucester, United Kingdom, [3]National Nuclear Laboratory, Bristol, United Kingdom

Late Poster Presentation

1267 Fatigue fracture behaviour of high strength steels under gaseous hydrogen

Dr Elina Saarivirta Huttunen[1], Pekka Pohjanne[1], Dr Pekka Moilanen[1], Dr Jouni Alhainan, Dr Supriya Nandy[1]
[1]VTT Technical Research Center of Finland Ltd, , Finland

1189

Pushing the limits of Coupled Extreme Environments during In-situ TEM

Professor Khalid Hattar

PS-12, Lecture Theater 2, august 29, 2024, 10:30 - 12:30

Background
In-situ TEM and STEM have pushed our understanding of the nanoscale and atomistic mechanisms active in materials exposed to thermal, mechanical, electrical, magnetic forces. Understanding at this length scale has been instrumental in the validation and refinement of many models developed to understand and predict materials degradation. In many ways, the ability of in-situ electron microscopy to explore a range of coupled extreme environments has become a path to an integrated materials science characterization toolbox. [1]

Methods
In the subfield of TEM with in-situ irradiation, it has been commonplace to combine in-situ ion irradiation with heating or cooling, mechanical loading, or both simultaneously. These advancements have been greatly advanced in the last decade or two with advancements in miniaturization that permit the inclusion of multiple probes into the same often small pole-piece gap, automation to permit the user to run multiple aspects of the experiment without assistance, and advanced manufacturing that permit costly development of parts for a specific microscope. One such example of a facility was the In-situ Ion Irradiation TEM (I3TEM) that was developed at Sandia National Laboratories to explore such coupled extreme environments. [2] This facility was unique in that it coupled two lasers into the I3TEM to permit both dynamic TEM (DTEM) imaging with 6 ns resolution and laser-based heating above 2000 °C for some samples. [3] Such examples raise the question of what the physical limit for is coupled in-situ TEM experiments and what are the limits set by historical presidents or engineering costs.

Results
Within the last year, the Tennessee Ion Beam Materials Laboratory (TIBML) has taken on the challenge of pushing the limit in coupled in-situ experiments in various extreme environments. This facility will be based on a JEOL 2100+ STEM with PyJEM compatibility. This microscope was chosen due to a combination of robust nature and ease of use. The high tilt pole-piece and LaB6 options were chosen to permit greatest access to the sample and excellent imaging of dislocation loop structures in two-beam and related imaging conditions, respectively. The JEOL 2100+ has already been modified by JEOL/IDES for the inclusion of a C0 lens for increased brightness, a laser port aimed at the electron gun for potential DTEM experiments in the future, a laser port for sample heating, and a port for ion optics coming in perpendicular to the electron optics. In addition, the microscope has been outfitted with a Gas Injection System (GIS) from Waviks, the ability to do Automated Crystallographic Orientation Mapping (ACOM) from Nanomegas, and real-time defect analysis via edge computing from Theia Scientific. The process for the development of this instrument, the current status of the microscope, and the planned vision for coupling it with 20 W 1064 nm laser, 20 W 532 nm laser, 20 kV ion source, and 3 MV tandem accelerator will be presented.

Conclusion
Similar to advancements in electron microscopy resolution resulting from advancements in aberration correction, advancements in miniaturization, automation, and advanced manufacturing have greatly increased the potential for various coupled in-situ TEM experiments. This work will discuss the physical limits of coupled in-situ experiments and compare them to the current

engineering limits. It will also highlight the current status of the Tennessee in-situ ion irradiation STEM that is being developed to explore these extreme coupled environments.

Figure: The Tennessee In-situ Ion Irradiation Scanning Transmission Electron Microscope with several of the already implemented and planned upgrades labeled.

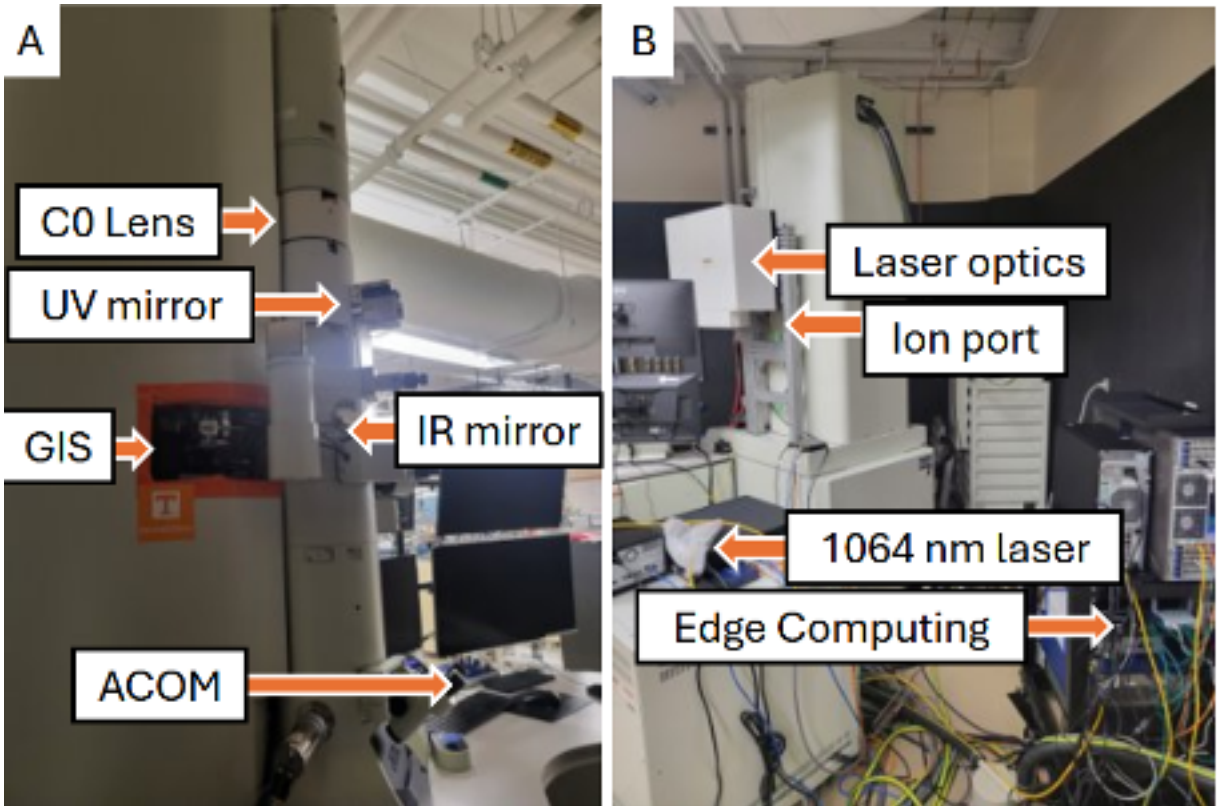

Keywords:

In-situ TEM; extreme environments; electron optics; ion optics

Reference:

[1] Robertson, Ian M., Christopher A. Schuh, John S. Vetrano, Nigel D. Browning, David P. Field, Dorte Juul Jensen, Michael K. Miller et al. "Towards an integrated materials characterization toolbox." Journal of Materials Research 26, no. 11 (2011): 1341-1383.
[2] Hattar, Khalid, Daniel Charles Bufford, and Daniel L. Buller. "Concurrent in situ ion irradiation transmission electron microscope." Nuclear Instruments and Methods in Physics Research Section B: Beam Interactions with Materials and Atoms 338 (2014): 56-65.
[3] Zhang, Yanwen, Miguel L. Crespillo, Haizhou Xue, Ke Jin, Chien-Hung Chen, CRISTIANO LINO Fontana, Joseph T. Graham, and William J. Weber. "New ion beam materials laboratory for materials modification and irradiation effects research." Nuclear Instruments and Methods in Physics Research Section B: Beam Interactions with Materials and Atoms 338 (2014): 19-30.
[4] Parrish, Riley J., Daniel C. Bufford, David M. Frazer, Caitlin A. Taylor, Jacob Gutierrez-Kolar, Daniel L. Buller, Brad L. Boyce, and Khalid Hattar. "Exploring coupled extreme environments via in-situ transmission electron microscopy." Microscopy Today 29, no. 1 (2021): 28-34
[5] Hattar, Khalid, and Katherine L. Jungjohann. "Possibility of an integrated transmission electron microscope: enabling complex in-situ experiments." Journal of Materials Science 56 (2021): 5309-5320.

105

Localized, anodic aluminum corrosion phenomena studied with electrochemical liquid phase electron microscopy

Morgan Binggeli Barbey[1], Prof. Vasiliki Tileli[1]
[1]Ecole polytechnique fédérale de Lausanne (EPFL), Lausanne, Switzerland

PS-12, Lecture Theater 2, august 29, 2024, 10:30 - 12:30

Local corrosion is a major concern for structural materials and it remains one of the most difficult defects to detect due to the submicron size of the local corrosion sites and the fact that they can be obscured by corrosion products [1]. The early stages of localized corrosion are the least understood and the most challenging to study as they occur stochastically at the solid-liquid interface on the nanometric scale [2]. With its combination of spatial resolution, temporal resolution, and analytical capability, electrochemical liquid-phase electron microscopy (ec-LPEM) has shown the potential to provide new insights into the understanding of localized corrosion phenomena [1], [3], [4]. Among these, Al corrosion in saline environments is a relatively well-studied phenomenon, allowing comparison of the ec-LPEM results with previous reports [2].

Commercially available transmission or scanning EM (SEM or TEM) stages were used to confine a liquid solution between two micro-electro-mechanical systems (MEMS) chips. To study Al corrosion using ec-LPEM, we have developed in-house microfabricated electrochemical chips containing one Al electrode and two Pt electrodes that can be electrically biased to perform in situ or operando electrochemical experiments. The three fabricated electrodes feature a symmetrical geometry to avoid local current density hotspots [5]. Potentiodynamic and galvanostatic electrochemical experiments were performed in situ for probing the corrosion of Al in chloride-containing electrolyte.

Linear sweep voltammetry (LSV) measurement was performed at a scan rate of 1 mV/s. The recorded electrochemical signal shows a plateau followed by a peak in the recorded current corresponding to the pitting potential. The recorded image sequence shows corrosion events occurring rapidly once the pitting potential is reached. The corrosion kinetics are found to be too fast for the time resolution of LPSEM. Thus, despite their widespread use in bulk systems, potentiodynamic techniques are not the most appropriate for recording localized corrosion phenomena using EM.

To achieve slower kinetics, galvanostatic control by means of chronopotentiometry (CP) measurements was performed at increasing current levels in the SEM. At the very low current of 1 nA, single pitting events were observed, whereas at the high end of the current range (50 nA), the corrosion was found to proceed rapidly with the simultaneous formation of a gaseous byproduct. Measurements performed at 1, 5 and 10 nA showed oscillations in the electrochemical signal, corresponding to the repassivation of the Al substrate with its naturally formed oxide. Two different corrosion shapes were observed: at low current (1, 5, and 10 nA), successive circular corrosion events occurred, whereas, at higher current densities (5, 10, 20, and 50 nA), fractal-shaped degradation occurred. This could indicate a kinetically dependent mechanism of Al corrosion.

The kinetic behavior of the anodic corrosion was calculated from the post-processed sequence of images taken over a 10-minute period. The processing consisted of 3D Gaussian blurring, median filtering, application of progressive image denoising algorithm, and segmentation of the images. This enabled the corroded area of the aluminum electrode to be determined for each image recorded. The calculated corrosion rates in the intermediate current range of 10 and 20 nA were found to be in good agreement with the theoretically determined oxidation rate of Al within a range of ±10%,

indicating the stability of the developed electrochemical system and the minimal effect of electron imaging on the corrosion mechanism.

Galvanostatic measurements at low applied current (5 nA) were also performed in the TEM. The real-time observations reveal that there is a distinct higher brightness that follows the corrosion front. This is indicative of gas formation (most likely H2) at the metal-liquid interface that is trapped during the process. It is noted that the recorded electrochemical signal did not match the one observed at the same applied current in the SEM, most likely due to electron beam-induced effects which are more pronounced at the scale of the TEM imaging.

In conclusion, we report the development of an electrochemical chip containing an Al electrode for real-time corrosion studies using ec-LPEM. Our methodology and findings can be applied to other electrochemical processes involving aluminum working electrodes, such as the cathode side of lithium-ion battery systems.

Keywords:

ec-LPEM, Al corrosion, pitting mechanisms

Reference:

S. W. Chee and M. G. Burke, Liq. Cell Electron Microsc. (2016).
G. S. Frankel and N. Sridhar, Mater. Today vol. 11 (2008).
F. M. Ross, Science (80-.). vol. 350 (2015).
A. Kosari et al., Corrosion vol. 76 (2020).
M. Binggeli et al., J. Electrochem. Soc. vol. 168 (2021).

218

Deformation mechanisms of inorganic fullerenes used as lubrication additives: an in situ TEM nanocompression study

Dr Sankar RK Pattamadai Sundaram[1], Dr Lucile Joly-Pottuz[1], Dr Pavel Afanasiev[2], Miss Marina Benmansour[3], Pr Fabrice Dassenoy[3], Pr Karine Masenelli-Varlot[1]
[1]MATEIS - INSA Lyon, Villeurbanne, France, [2]IRCELYON - UCBL, Villeurbanne, France, [3]LTDS - ECL, Ecully, France

PS-12, Lecture Theater 2, august 29, 2024, 10:30 - 12:30

Energy saving is a crucial point to hinder environmental issues. Lubrication of systems, especially engines, have been improved but further developments are still mandatory. Energy loss and wear of moving parts have to be decreased. Inorganic fullerene-like – IF- nanoparticles made up of metal disulphides MoS2, WS2 are considered as promising candidates for anti-wear and anti-friction additives. It was first thought that their round shape will allow them to act as small ball bearings inside the contact but an exfoliation mechanism has been observed [1,2]. This exfoliation leads to the formation of lubricant sheets in the contact area. TEM nanocompression experiments allowed to observe this exfoliation in situ [3]. Depending on the synthesis conditions, fullerenes can present a well-defined onion-like structure with a hollow center or can be composed of not well aligned MoS2 sheets without hollow center. This difference of structure leads to different tribological results. To better understand this discrepancy of behavior, in situ TEM nanocompression/nanofriction experiments were performed on both types of structures to mimic what can happen in the tribological contact. Furthermore, the chemistry of the IF nanoparticles may have an impact. In situ testing experiments were performed under vacuum and under oxygen to monitor the effect of oxygen on their behaviour inside the tribological contact.

MoS2 nanoparticles with controlled sizes and structures were prepared by exposing sheelites MoMO4¬ nano particles to a H2S-CCl4-Ar gas mixture [4]. After dispersion in a solvent by sonication, they were deposited on a silicon substrate mounted on a copper pallet attached to the Bruker/ Hysitron PI-95 TEM holder. In situ compression and friction behaviour of MoS2 nanoparticles with different level of crystallinity (poor, medium, high) under vacuum and oxygen atmosphere were performed, in an aberration corrected environmental TEM microscope (FEI Titan ETEM). Poorly crystalline fullerenes present a structure with a random orientation of MoS2 sheets. Medium and highly crystalline fullerenes present an onion-like structure, highly crystallinity having less defects. The structural changes of nanoparticles under compression and/or during friction were imaged in TEM bright field mode with a 25 frames/s acquisition rate. A precise processing, by following the change of the particle shape and the presence of shear, was determined to fully characterize and understand the deformation mechanism. Observations were linked to the force-displacement curve.

Comparison of compression experiments for the different crystallinities present different deformation mechansims. For the low crystallinity sample, orientation of the sheets perpendicular to the compression axis is observed during compression and shearing (see figure). For onion-like medium crystalline particles, buckling of the inner shell initiates the deformation, while it is not observed in highly crystalline ones. The buckling may be due to the presence of defects. The onion-like morphology leads to a large amount of elasticity and their plastic deformation to orientation of planes perpendicular to load direction. The amount of elasticity, the mechanism of deformation initiation and the forces differ according to morphology, while at the end MoS2 sheets align to the perpendicular direction of applied load.

In situ nanocompression experiments in ETEM are useful to observe the exfoliation mechanisms of fullerenes. It was already known that the lubrication mechanism of fullerenes is based on their exfoliation. The interest here is to be able to observe the exfoliation mechanism and to compare the behavior of fullerenes with different crystallinity. A different behavior has been observed depending on their crystallinity, with both mechanisms leading to the formation of MoS2 sheets in the lubricated contact.

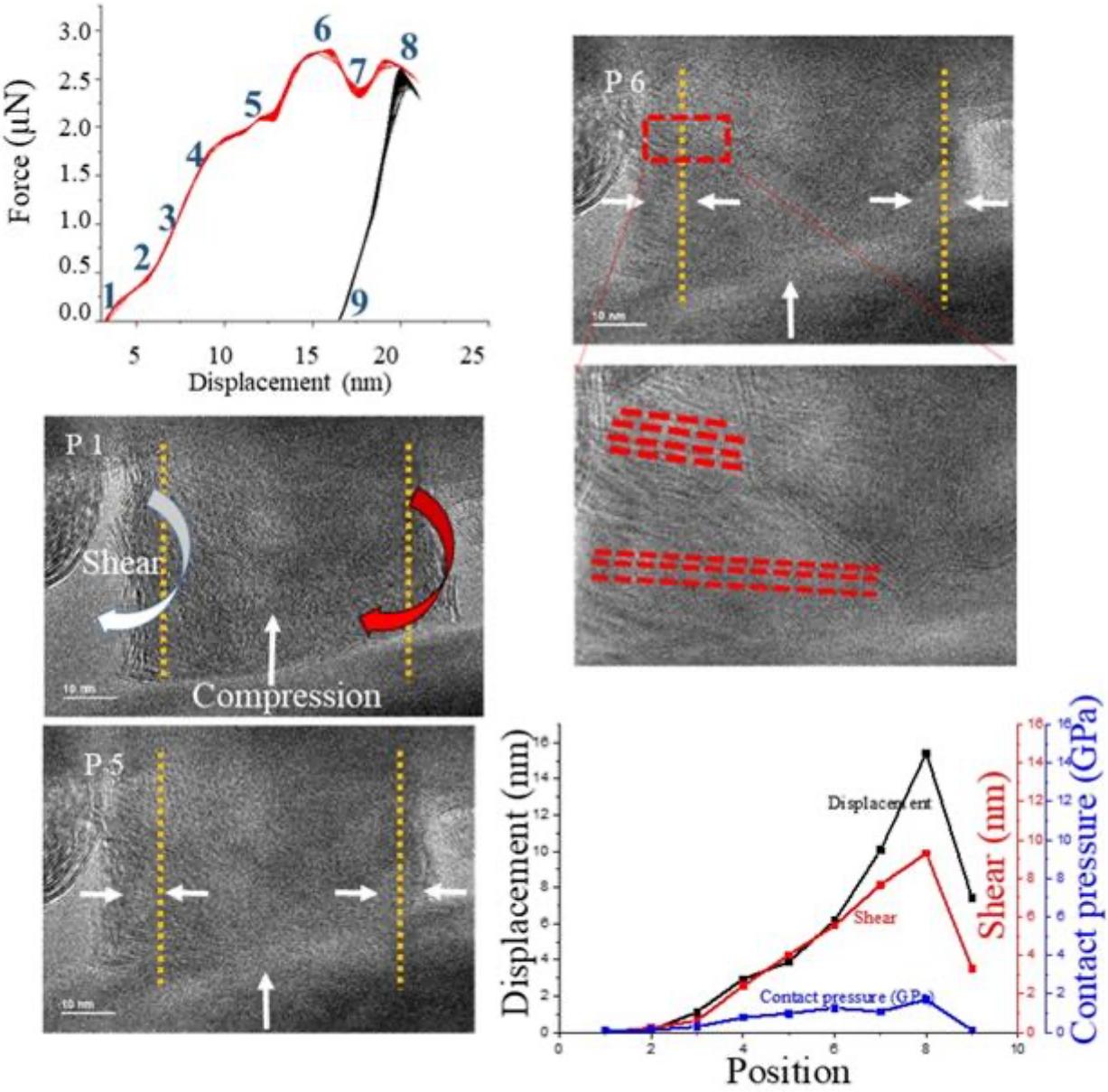

Keywords:

In-situ
ETEM
Nanocompression
Nanofriction

Reference:

[1] L. Cizaire et al., Surf Coat Tech 160, 282 (2002),
[2] L. Joly-Pottuz et al., Trib Lett 18, 477 (2005)
[3] I. Lahouji et al., Tribology Letters 43, 133, (2011)
[4] P. Afanasiev, Appl. Catal. B: Environmental, 227, 44 (2018)

497

In-situ nucleation of silicon particles using environmental transmission electron microscopy

Dr Lucian Roiban[1], Dr. Cynthia Cibaka-Ndaya[2], Dr. Kevin O'Connor[3], M. Emmanuel Opeyemi Idowu[2], Professor Jonhatan G.-C. Veinot[3], Dr. Glenna L. Drisko[2]
[1]INSA Lyon, Université Claude Bernard Lyon 1, CNRS, MATEIS, UMR5510, Villeurbanne, France, [2]ICMCB, UMR 5026, CNRS, Univ. Bordeaux, Bordeaux INP, Pessac F-33600, France, [3]Department of Chemistry, The University of Alberta, Edmonton, Canada

PS-12, Lecture Theater 2, august 29, 2024, 10:30 - 12:30

Background incl. aims

Silicon (Si) particles are excellent candidates for the development of optical metamaterials with high scattering efficiency for applications in anti-counterfeiting, nonlinear nanophotonics and enhanced Raman scattering. An optimized synthesis method that allows the fabrication of Si nanoparticles with resonant properties that depend on their size, crystallinity and density would open the way to the large-scale production of such so-called metamaterials. Today, one of the most promising synthesis methods is the thermal disproportionation of hydrogen silsesquioxane (HSQ), which produces resonant silicon particles with the desired criteria. However, the disproportionation of HSQ occurs at very high temperatures and the particles produced are polydisperse in size, requiring a separation process to obtain a monodisperse particle.
In this work, the nucleation and growth of Si particles from the thermal disproportionation of HSQ and the formation of silicon nanoparticles with diameters up to 70 nm were investigated. Advanced in situ environmental transmission electron microscopy (ETEM) was used to directly observe the formation of Si particles from HSQ to resonant particles at high temperature under 20 mbar of gas pressure.

Methods
In situ experiments were performed using a FEI ETEM Titan 80-300 environmental microscope operating at 300 kV equipped with a OneView camera from Gatan. HSQ grains were crushed in a mortar and then dispersed in 2-propanol, a drop of the highly dilute dispersion was placed on a Si3N4 chip compatible with DENSsolutions Wildfire sample holder then dried. The experiments were performed under a gas pressure of around 20 mbar. The gas employed was argon or a mixture of N2 - H2 (95%-5%). The temperature was raised from RT to 800 °C at a rate of 10 °C/sec with about 2 min of plateau every 100 °C. From 850 °C to 1300 °C, the temperature was increased by step of 50 °C, at a rate of 10 °C/sec with plateaus of about 20 min – 1h at 900 °C, 1000 °C, 1100 °C, 1200 °C and 1300 °C in order to record images and videos of the nucleation and growth processes. Cooling of the sample to RT was carried out by step of 100 °C at a rate of -10 °C/sec.

Results
As expected, the thermal decomposition of HSQ was found to begin at temperatures above 1000°C. Once the Si crystalline nuclei are formed, two main growth processes are observed, including particle-particle coalescence and, more surprisingly, particle displacement through the matrix, leaving traces through the HSQ matrix due to interfacial chemical reactions. At 1000°C, small particle nuclei of about 1 nm are visible, then with increasing temperature to 1200°C, particles of 7-11 nm are observed. Then these particles begin to coalesce, indicating high mobility within the system, and the particles formed have a larger projected diameter (Figure 1a).
The second growth mechanism observed shows that the particles move through the sample by changing shape and growing up to 70-80 nm (Figure 1b). They show a liquid-like behavior, are very

mobile and change shape rapidly. This liquid-like behavior below the typical melting point of silicon is attributed to a beam effect lowering the melting point during in-situ observation.
The in-situ experiments were complemented by in-situ XRD measurements up to 1200 °C, demonstrating a solid-state growth mode below the melting point of Si. [1,2]

Conclusion
This study was conducted under extreme conditions using an ETEM under 20 mbars of gas and at 1300°C and helped to illuminate the growth mechanism of Si nanoparticles from a silicon rich oxide precursor. It was found that crystalline Si domains grow easily in the solid state starting from 1000°C. For the first time, a highly malleable and mobile phase was observed in real time, suggesting an intermediate liquid-like behavior that facilitates particle growth. Growth processes by coalescing and moving within the matrix after the crystallization were identified. This study was complemented by an ex-situ investigation of the role of the reducing atmosphere in the disproportionation reaction.

Figure 1: Si particles formed after thermal decomposition of HSQ grew by two different mechanisms: a) Particles coalescence, the Si particles have high mobility at 1200°C and during the encounter they form larger nanoparticles. b) At 1300°C the particles have liquid like behavior with high mobility moving through the matrix while growing.

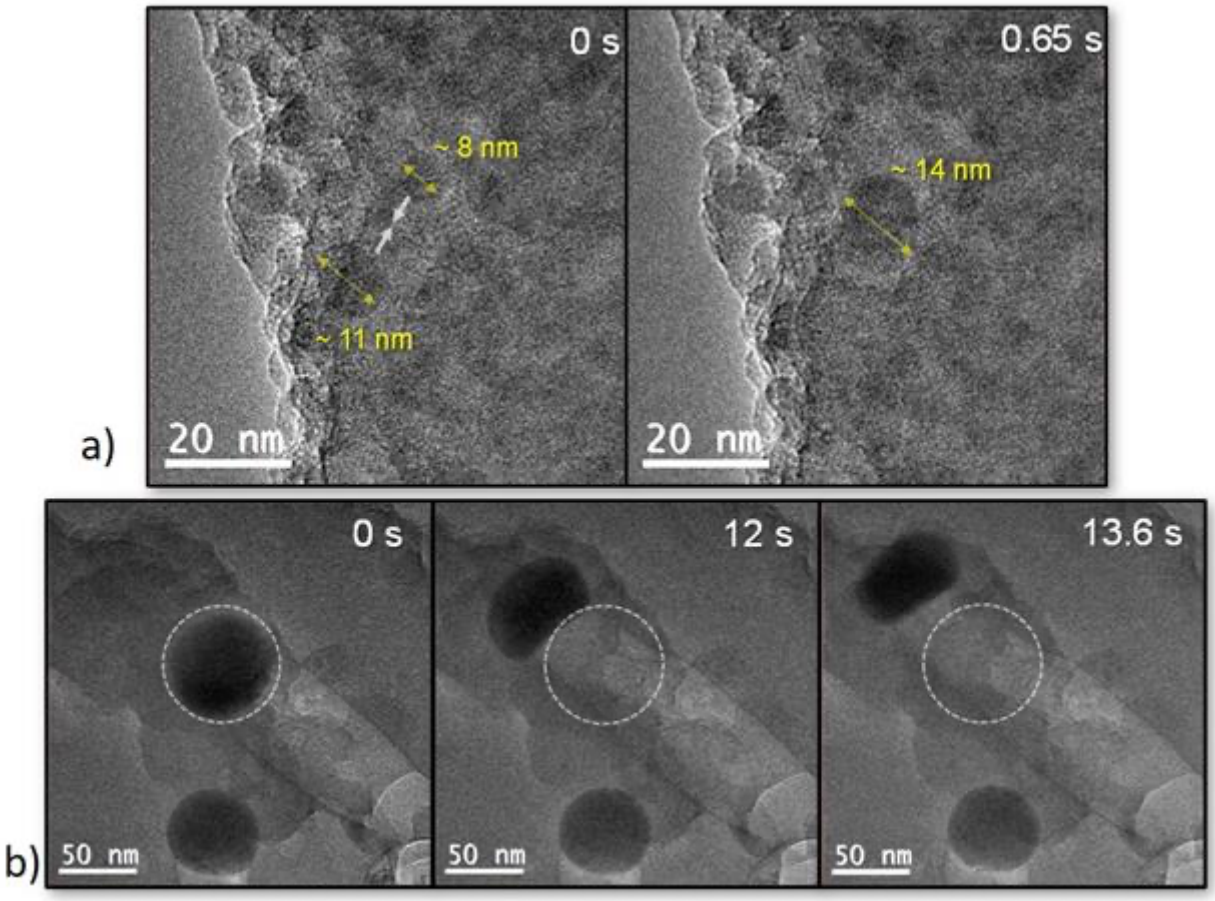

Keywords:

In-situ, HSQ hdisproportionation, Si synthesis

Reference:

[1] Cibaka et al. Chem. Mater. 2023, 35, 20, 8551–8560
[2] the Consortium Lyon Saint-Etienne de Microscopie (CLYM) is acknowledged for microscope access, the European Research Council (ERC) under the European Union'sHorizon 2020 research, innovation program (Scatter, Grant agreement no. 948319) and METSA network are acknowledged for the financial support

522

Study of nuclear materials for silicon carbide composite fuel claddings via STEM, EDX and EELS

Phd Student Hector Guerra Yanez[1], PhD Student Andrea Stinchelli[2,3], Doctor Fabio Di Fonzo[3], Professor Per O.Å. Persson[1]
[1]Department of Physics, Chemistry and Biology, University of Linköping, Linköping, Sweden, [2]Department of Energy, Politecnico di Milano, Milan, Italy, [3]X-nano s.r.l., Milan, Italy

PS-12, Lecture Theater 2, august 29, 2024, 10:30 - 12:30

Background incl. aims
Silicon carbide composites (SiC/SiC) are promising materials for fuel claddings in light-water reactors as their thermal, chemical and mechanical stability extend to very high temperatures, granting longer coping time in case of a loss-of-coolant accident. These materials would potentially allow to claim a power plant back even after many hours without active cooling of the core [1,2]. Despite their excellent performance under accidental conditions, during normal operating conditions, SiC/SiC composites are oxidized by the cooling water, forming silica (SiO_2). To prevent this, the application of a protective coating over the cladding is proposed. In this study, yttrium aluminum garnet (YAG) and chromium-doped yttrium oxide (Cr:Y_2O_3), deposited with pulsed laser deposition (PLD), were studied by scanning transmission electron microscopy (STEM). The coatings were observed before and after thermal treatment at temperatures resembling severe loss-of-coolant accidents.
Methods
Four samples were studied: 1) pristine YAG deposited on a silicon substrate; 2) YAG deposited on a stainless steel substrate that was annealed in air after deposition at 900 °C for 1 hour; 3) pristine Cr:Y_2O_3 deposited on a silicon substrate; and finally 4) Y_2O_3 with the same amount of Cr_2O_3 deposited on a zircalloy substrate and annealed at 1300 °C for 1 hour.
Electron-transparent samples for STEM were prepared by traditional low-angle Ar ion milling and by focused ion beam (FIB). The microstructure was investigated in the Linköping double corrected, monochromated FEI Titan3 60-300, operated at 300 kV. Energy dispersive x-ray spectroscopy (EDX) and electron energy loss spectroscopy (EELS) were employed to identify elements and density variations in the samples.
Results
STEM imaging of the samples shows that sample 1) is amorphous, however, apparent layering with an approximate period of 20 nm was observed in the sample. EELS spectrum imaging was performed to discern if the layering occurred as a consequence of elemental inhomogeneities or because of density variations within the coating, confirming the former. After annealing, the YAG assumed a crystalline nature with ~1 µm equiaxed grains (sample 2). The grain boundaries accommodate large voids and the original layers were removed, as can be observed in the graphic. The presence of these grain boundaries decorated by voids suggests that this material may not function as a diffusion barrier for water.
Sample 3) displays a predominantly amorphous structure, although crystalline nanoparticles are randomly distributed in the amorphous matrix. After annealing (sample 4), this coating presents different microstructures near the substrate and near the surface. The film has crystallized, and near the substrate, the film exhibits a dense structure. In contrast, the surface near region also exhibits a crystalline nature, although the grain boundaries appear to be porous and disordered. The origin of this presumably owes to chromium oxide segregating at the grain boundaries and evaporating during the annealing process, leaving underdense boundaries behind that become swift routes for further chromium diffusion.
This is supported by the concentration of chromium, which is notably higher in the region near the substrate compared to near the surface, as measured by EDX. The interface between the two

different microstructures shows apparent particles of segregated chromium. These presumably originate from migrating chromium that condenses into nanoparticles during the rapid cooldown. The gradual migration of chromium that occurs during annealing in the $Cr:Y_2O_3$ can help protect the integrity, or delay catastrophic failure, of the system as the inner phase maintains a diffusion barrier and effectively protects the fuel cladding.

Conclusion

This study shows that $Cr:Y_2O_3$ is a valid alternative material as a coating for SiC/SiC composites. This can be affirmed since the material acquires a microstructure that is gradually consumed during high-temperature processing.

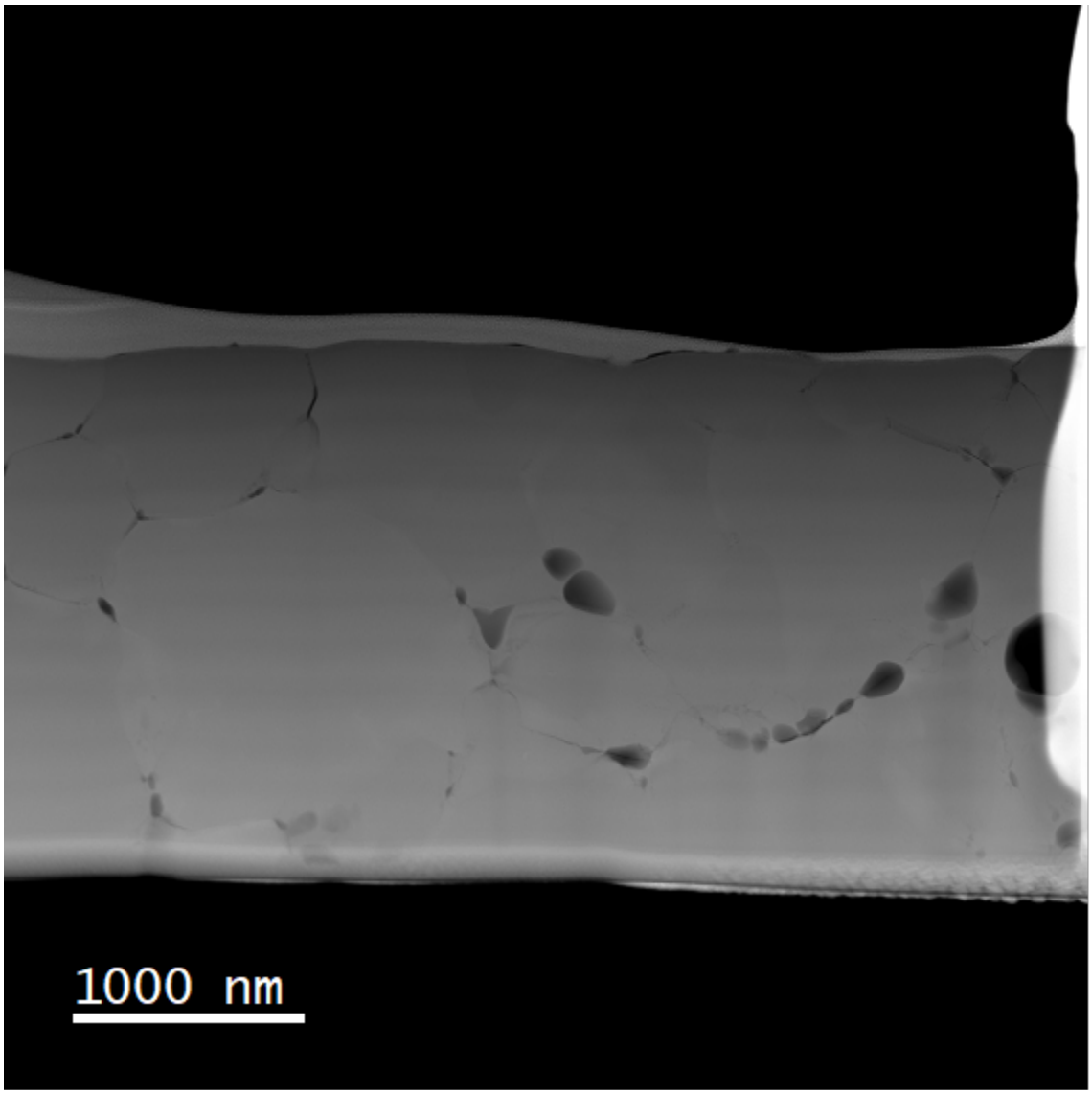

Keywords:

Nuclear materials EELS STEM EDX

Reference:

[1] K. Barrett, S. Bragg-Sitton, D. Galicki, Advanced LWR Nuclear Fuel Cladding System Development Trade-off Study, INL/EXT-12-27090, September 2012.

[2] Steinbrueck, M.; Grosse, M.; Stegmaier, U.; Braun, J.; Lorrette, C. High-Temperature Oxidation of Silicon Carbide Composites for Nuclear Applications; TopFuel: Santander, Spain, 2021.

763

In-situ TEM ion irradiation studies of layered MAX phase materials

Mrs Eman Al Ruqeishi[1], Max Rigby-Bell[2], Graeme Greaves[3], Alexander Eggeman[1], Sarah Haigh[1]
[1]University of Manchester, Manchester, United Kingdom, [2]UK Atomic Energy Authority, Abingdon, United Kingdom, [3]University of Huddersfield, Huddersfield, United Kingdom

PS-12, Lecture Theater 2, august 29, 2024, 10:30 - 12:30

Materials in the core of a nuclear reactor are exposed to severe environments, particularly in future Generation IV nuclear systems, which perform in environments with high temperatures and high fluxes of fast neutrons, causing hundreds of displacements per atom (dpa) as well as substantial helium (He) doping by nuclear transmutation. MAX phases have attracted attention for their potential in nuclear materials due to their demonstration of high stabilities [1]. This study investigates the impact of sequential irradiation with light and heavy ion irradiation of MAX phases, specifically comparing the irradiation induced changes in Ti_3SiC_2 and Ti_3AlC_2. Cross sections of both MAX phases were prepared using focused ion beam milling. These were irradiated inside the MIAMI transmission electron microscopy (TEM), in situ TEM irradiation facility [2], first with 75 keV He+ ions at a dose of 2.6 x 10^{16} ions/cm² up to 3 dpa, and then with 600 keV Ar^{2}+ ions with a total fluence of 9.2 x 10^{16} ions/cm² up to 50 dpa, at both room temperature and 350°C. TEM imaging and diffraction are used during in-situ ion irradiation for direct observation of the microstructural and unit cell evolution. In-situ TEM observations indicate that both materials retained their crystal structures for the full irradiation dose. There was no observation of significant amorphization, phase transformations, He bubbles, or decomposition. The helium irradiation-induced damage, manifested as point defects, increases with damage level (dpa), resulting in anisotropic changes in lattice parameters in both structures up to ~ 9% and at both room temperature and irradiated temperatures. Interestingly, a significant recovery towards the as-synthesized unit cell parameters was observed post-irradiation within a few days of ambient storage at room temperature. Subsequent irradiation then followed similar irradiation damage profiles as the original pristine MAX phase with lattice parameter changes up to ~ 8% without significant amorphization, followed by another room temperature structural recovery when the irradiation is stopped. This observation of exceptional irradiation stability combined with room temperature recovery provides new evidence of the potential of MAX phases in protective coatings for nuclear applications and for radiation sensing and detection.

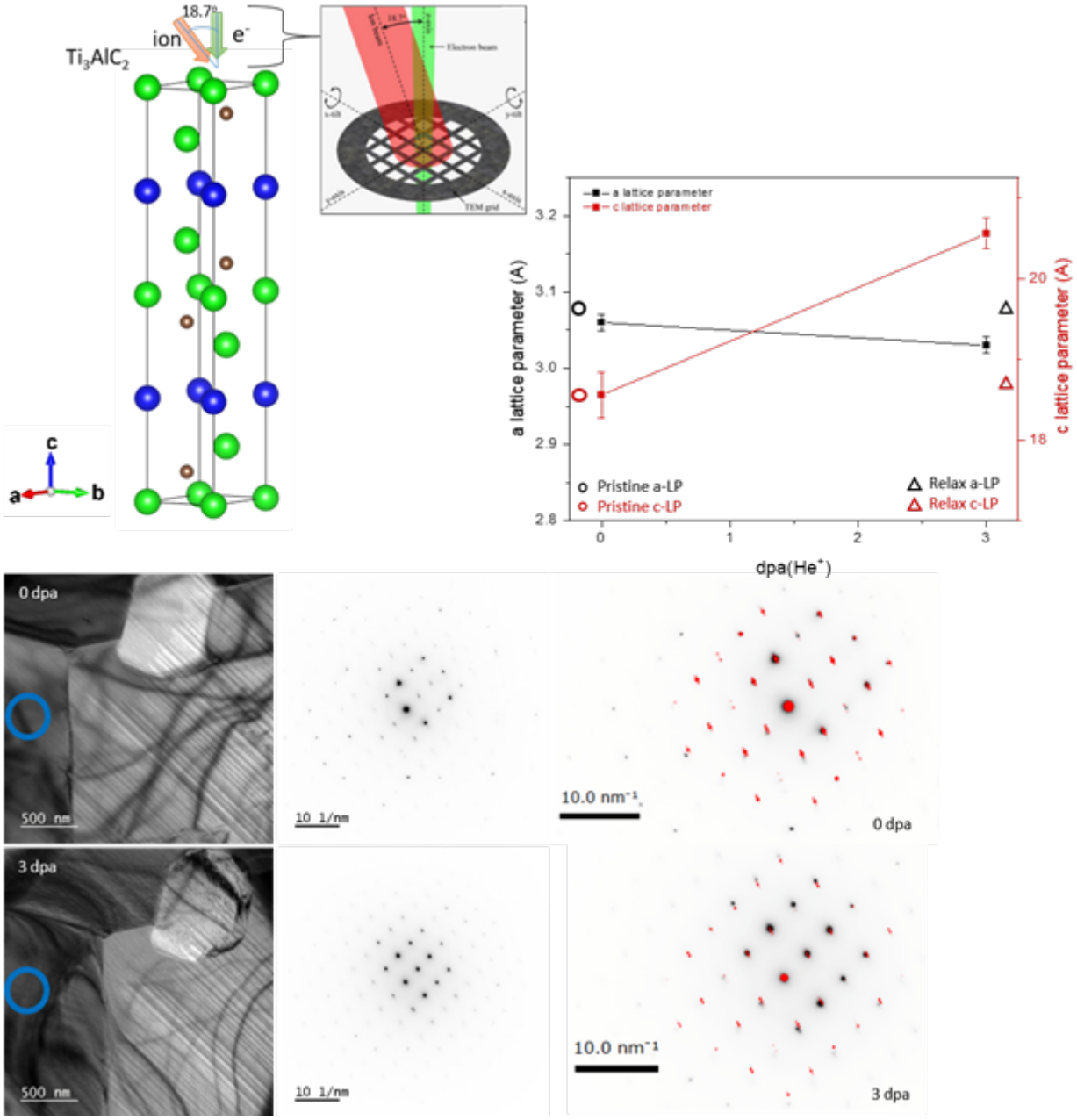

Keywords:

In-situ radiation, MAX-phases, radiation tolerance.

Reference:

[1] Barsoum, M. W. (2000). The MN+ 1AXN phases: A new class of solids: Thermodynamically stable nanolaminates. Progress in solid state chemistry, 201--281.
[2] Greaves, G. M. (2019). New microscope and ion accelerators for materials investigations (MIAMI-2) system at the University of Huddersfield. Nuclear Instruments and Methods in Physics Research Section A: Accelerators, Spectrometers, Detectors and Associated Equipment, 931, 37-43.

1029

Correlative microscopy of creep cavitation in steels using image processing of SEM, FIB-XeF2 and EBSD

Dr Tomas Martin[1], Dr Siqi He[1], Ms Eirini Gallioupolou[1], Mr Peter Thomas[1], Mr Edward Horton[1], Mr Michael Salvini[1], Dr Nicolo Grilli[1], Professor David Knowles[1], Professor Mahmoud Mostafavi[1], Professor Peter Flewitt[1]
[1]University of Bristol, Bristol, United Kingdom

PS-12, Lecture Theater 2, august 29, 2024, 10:30 - 12:30

Background incl. aims
Creep cavitation is an important degradation mechanism in metal alloys at high temperatures, such as in aerospace engines, gas turbines and nuclear fission and fusion reactors. During operation, metal components such as 316H stainless steel boiler headers are subjected to elevated temperatures and stresses, particularly close to weldments and geometrical features [1]. Over extended service lifetimes, these temperatures and stresses result in vacancy and dislocation movement that can gradually accumulate at microstructural features in the alloy, resulting in the formation of creep cavities that can develop into cracks and eventual failure of the component. This mechanism starts at the microstructural level, and to understand the process, it is important that the evolution of creep cavitation from nucleation to growth is characterized using advanced microscopy.
Previous work [1] has shown that in ex-service material after 65,000 hours in service in an advanced gas-cooled nuclear reactor (AGR) at 490°C–530°C, the heat-affected zone close to a weld in a 316H boiler header became extensively cavitated as a result of creep cavitation. Detailed microstructural analysis using scanning electron microscopy (SEM), electron backscatter diffraction (EBSD) and transmission electron microscopy (TEM) showed that cavities in this material were correlated with precipitation on the grain boundaries of the steel, most significantly at the interface between $M_{23}C_6$ carbides and ferrite which had formed during thermal ageing. This detailed understanding of the interaction between microstructure and creep cavitation is essential to determine component lifetimes and design new creep-resistant materials.
However, to fully understand the interactions between creep damage and microstructure, it is beneficial to characterize this interaction over larger regions of an affected material, whilst retaining the high resolution structural, crystallographic and elemental information of individual microscopy images. In this work, we present a new methodology that combines these techniques with image processing to provide spatially-identified datasets of creep cavities, precipitation and grain structure with nanometre resolution, but across millimeter length scales of a component.
Methods
Type 316H austenitic stainless steel material was removed from a boiler component, initially service-exposed for 65,000 hours at 490°C–530°C in an AGR. Material was extracted away from high stress regions of the component and was characterized to ensure it had thermally-aged microstructure but no existing creep cavitation. The material was subsequently machined into a notched creep specimen with a gauge length of 40mm, a notch radius of 6mm and a notch acuity of 5. The creep specimen was subjected to 25 cycles of tensile stress relaxation at an initial net section stress of 390 MPa and a temperature of 550°C, and then allowed to relax in pure strain control. After testing, the crept specimen was sectioned axially, ground and polished using diamond slurry and vibropolishing to an EBSD-quality mirror finish.
An area of 3.2x1.2 mm across the centre of the sectioned specimen around the notch was imaged using 162 backscattered electron (BSE) images with a 30% overlap between neighbouring images using a Zeiss SigmaHD FEG-SEM, as well as EBSD and FIB-XeF_2 imaging across the same region. The FIB-XeF_2 imaging approach used a ThermoFisher Scios2 focused ion beam instrument, and utilized a XeF_2 gas injection system to enhance contrast between the metal matrix and precipitates, as

described in [2]. The software package Dragonfly (Object Research Systems Inc, Montreal, Canada) was used for post-image processing, segmenting the BSE images to identify cavities and the FIB-XeF_2 images to identify precipitates using an Otsu threshold selection methodology [3]. EBSD data was corrected using an in-house Matlab script and all three datasets were then overlaid to enable correlation between the cavity, precipitate and grain boundary information across the entire 3.2x1.2mm region to be characterized statistically. Further detail on the methodology can be found in [4].

Results

The graphic shows an example of this correlative workflow. Figure (a) shows a stitched FIB-XeF_2 image of a 3.2 mm x 1.2 mm region of the creep specimen, with the notch at the left of the image. The stiched image comprises 32 individual FIB-XeF_2 images, which along with the 162 BSE images were image processed to identify creep cavities, cracks and precipiates by grayscale contrast and morphology. Two example frames with image processing are shown in (b) and (c), where yellow represents identifed $M_{23}C_6$ carbide precipitates (verified by transmission electron microscopy diffraction) and blue represens creep damage. (d) shows the statistical overlay of the identified precipitates in yellow with the grain boundary locations obtained by EBSD in blue, across the entire sampled region. Similar maps of damage were also obtained. The statistical analysis of these data described in full in [4] showed that damage showed very little correlation with grain-to-grain differences in Schmid factor (which many computational models of creep assume to be a key factor in damage location), but in this material precipitation, grain boundary angle and localised strain (as indicated by the kernal average misorientation in the EBSD data) showed much clearer correlation with damage, indicating that in this material the trapping sites at grain boundary carbide precipitates are the primary initation sites for creep damage.

Conclusion

Creep cavitation is a complex degradation mechanism, which starts at the atomic or nanometre scale and over extended times can build to failure of entire components. The methodology presented here shows the effectiveness of advanced microscopy combined with image processing to statistically correlate microstructural features with damage locations in crept material, enabling much better understanding over large areas of the contributing factors to this process.

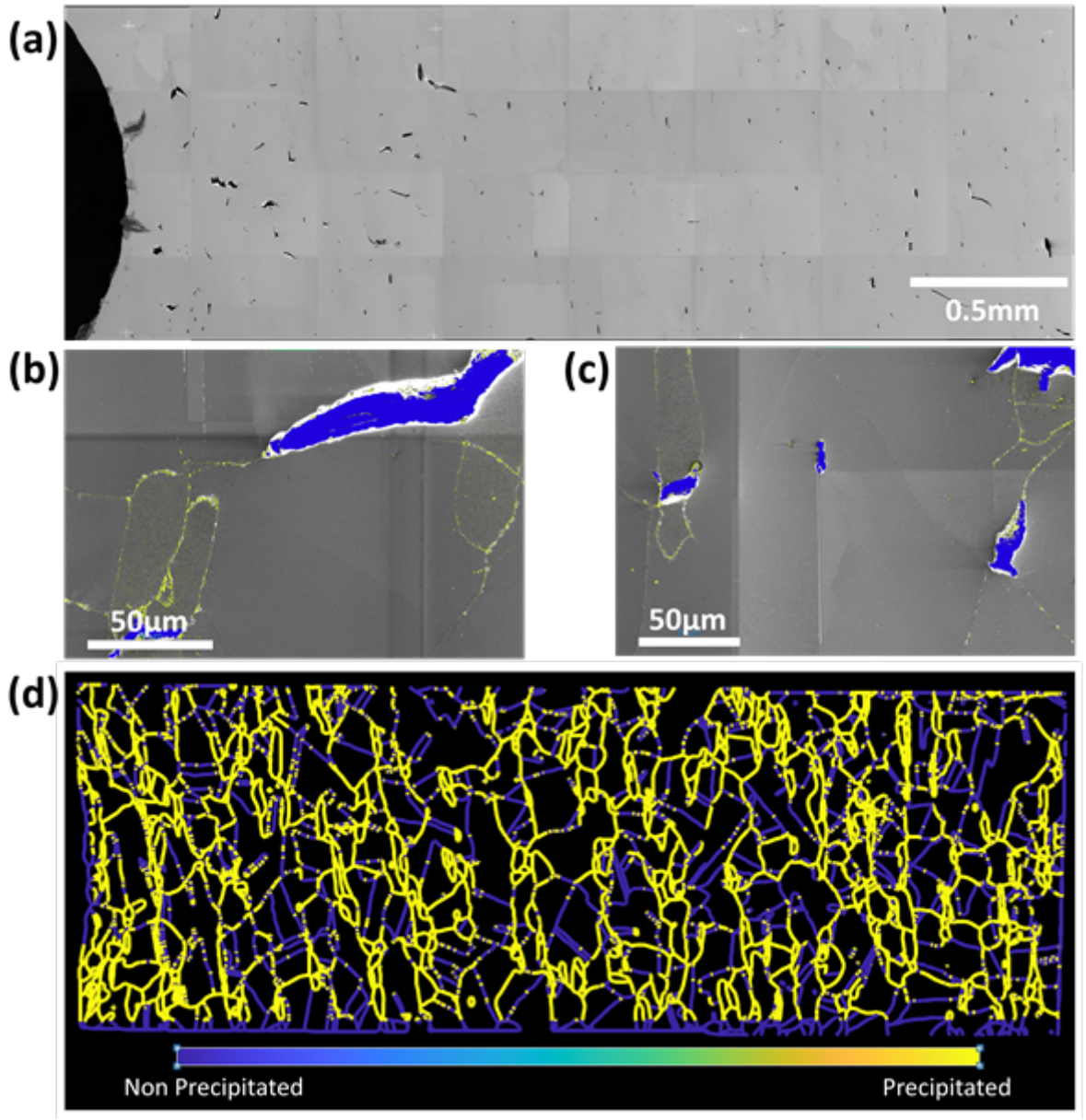

Keywords:

Creep, steel, correlative microscopy

Reference:

[1] S. He, H. Shang, A.F.- Caballero, A.D. Warren, D.M. Knowles, P.D. Flewitt and T.L. Martin, The role of grain boundary ferrite evolution and thermal aging on creep cavitation of Type 316H austenitic stainless steel, Materials Science and Engineering: A, 807, 140859 (2021) DOI:10.1016/j.msea.2021.140859

[2] P.J. Thomas, M. Zimina, A. Shin, J. Pearson, P.E.J. Flewitt, T.L. Martin, Microstructural Evolution due to CO2 Oxidation and Carburisation in Fe9Cr1Mo Steel, in: Transactions of the SMiRT 27, (2024).

[3] N. Otsu, A Threshold Selection Method from Gray-Level Histograms, IEEE Transactions on Systems, Man, and Cybernetics 9 (1979) 62–66. DOI:10.1109/TSMC.1979.4310076.

[4] S. He, E. Horton, S. Moore, E. Galliopoulou, P.J. Thomas, A. Fernandez-Caballero, E. Elmukashfi, M. Salvini, M. Mostafavi, D.M. Knowles, P.E.J. Flewitt, T.L. Martin, A correlative approach to evaluating the links between local microstructural parameters and creep initiated cavities, Materials & Design (2024) 112905. DOI:10.1016/j.matdes.2024.112905.

300

In situ scanning precession electron diffraction study of chemo-mechanical interactions during Zr oxidation

Dr. Dan Zhou[2,3], Yongwen Sun[1], Dr. Ying Han[1], Dr. H. Hugo Perez Garza[3], Dr. Alejandro Gomez Perez[4], Dr. Athanassios S. Galanis[4], Dr. Stavros Nicolopoulos[4], Prof. Dr. Yang Yang[1]
[1]Department of Engineering Science and Mechanics and Materials Research Institute, The Pennsylvania State University, University Park, PA, 16802, United States, [2]Leibniz Institute for Crystal Growth, Berlin, 12489, Germany, [3]DENSsolutions B.V., Delft, 2628 ZD, Netherlands, [4]NanoMegas SPRL, Brussels, 1050, Belgium

Poster Group 2

Background
Zirconium (Zr)-based alloys, serving as cladding materials for nuclear reactor fuel, are susceptible to oxidation under harsh operation conditions. The stress redistribution and strain anisotropy induced by oxidation could elevate the risk of reactor failure and limit the operational economy. Efficient in situ strain mapping techniques are crucial for elucidating the fundamental mechanisms of oxidation processes and advancing the development of more sustainable cladding materials to ensure the safety of nuclear reactor operations. Recent developments of MEMS-based NanoReactors enable in situ TEM studies of reactions at temperatures up to 1000 °C and pressures up to 2 bar. The integration of a vaporizer extends in situ gas phase TEM from dry to humidified gas environments. Specifically, for Zr-based alloys, these innovations facilitate oxidation studies under both dry oxygen and water vapor conditions.
In this work, we pioneer an in situ strain mapping methodology to explore oxidation processes in zirconium by integrating four-dimensional scanning transmission electron microscopy (4D-STEM), MEMS gas-cell holder, precession electron microscopy (PED), and direct electron detector (DED). Central to our successful strain mapping is achieving optimal signal-to-noise ratio within nanobeam electron diffraction patterns (NBEDs).
Methods
A DENSsolutions' in situ gas phase TEM system Climate G+ and a FEI Tecnai 20 with NanoMEGAS ASTAR and Topspin platform were used in this work. The Zr sample was first cut and thinned by the focused ion beam (FIB) and then transferred to the Climate nano-reactor.
Results
Figure 1 depicts the influence of precession on a representative nanobeam electron diffraction (NBED) pattern, an area strain mapping, and an area orientation mapping by toggling precession off and on over the identical region on the Zr sample. The application of precession visibly reduces their sensitivity to the sample thickness and its local bending, increases the number of higher-order reflections, and improves the signal-to-noise ratio. Therefore, it enhances the straining mapping precision and orientation reliability.
A comparison between in situ gas-cell 4D-STEM mapping results using PED at Argon gas pressures of 0 mbar and 500 mbar tells although both PED patterns retain similarity to kinematic ones, the increased pressure lowers the signal-to-noise ratio. Consequently, the reliability of the strain mapping at higher pressure is reduced, as marked by the additional noise present in the strain mapping.
Further details on how we tackle the challenges of FIB sample preparation on a gas cell, the conflict of sample evolution process in a few seconds and SPED data acquisition in a few minutes and so on will be presented on site.
Conclusion
Our approach facilitates precise, nanometer-scale strain mapping across a large field of view during zirconium oxidation. This developed workflow has significant implications for corrosion studies,

offering profound insights into the chemo-mechanical evolutions in materials subject to harsh environments.

Figure caption

Figure 1 Comparison of precession's importance in enhancing the quality of diffraction pattern (left), hydrostatic strain map (middle) and ASTAR orientation map + reliability (right).

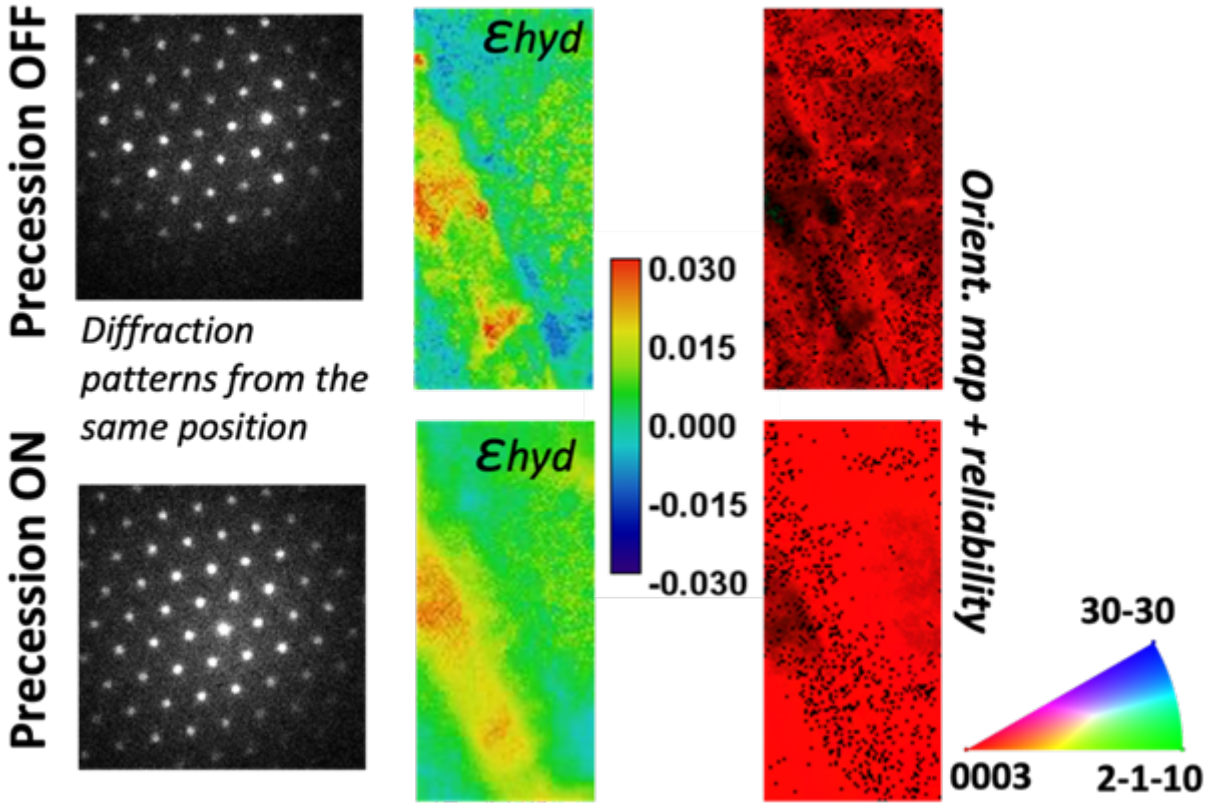

Keywords:

In situ, SPED, strain mapping

Reference:

No

643

In- and ex-situ implantation of helium to characterise faults in titanium beryllide

Dr Jo Sharp[1], Dr Slava Kuksenko[2], Dr Ramil Gaisin[3], Professor Jonathan Hinks[1], Dr Graeme Greaves[1], Professor Stephen Donnelly[1], Professor Pavel Vladimirov[3]
[1]University of Huddersfield, Huddersfield, United Kingdom, [2]UKAEA, Culham, United Kingdom, [3]Karlsruhe Institute of Technology, Karlsruhe, Germany

Poster Group 2

Background incl. aims
Transition metal beryllides, MBe_{12}, are an important material class in tokamak fusion reactors for use in tritium breeder modules as a neutron multiplier to maintain the refuelling cycle. During the neutron multiplying reaction chain, helium and tritium are also produced as well as knock-on radiation damage. Beryllium metal is a commonly used candidate neutron multiplier but develops large helium bubbles at breeder module operating temperatures which retain tritium on their inner surfaces (Zimber, et al., 2023), which complicates end-of-life recycling and would be a radiation and explosion hazard in an accident scenario. Titanium beryllide retains less tritium and is tougher (Kim, et al., 2021), so has been chosen as a candidate neutron breeder for EU-DEMO and JA-DEMO. There are still many material unknowns, however; what crystal defects develop, what do they do at high temperature, and how do helium and tritium/hydrogen behave in the microstructure?

Methods
In this study we used the University of Huddersfield's MIAMI-2 ion beam/TEM to implant 300kV He+ ions into 2µm thick sections ("bulk ex situ" sections for the purposes of containing the He peak) of TiBe12 at temperatures 387°C, 480°C, 600°C and 900°C to fluence of 10^{17} ions/cm². From this energy we expect a He peak approximately 900nm under the surface. We then re-sectioned the samples to produce cross sections parallel to the irradiation direction, with the He peak present as a horizontal band of helium approximately 900nm down the re-section. To begin investigating the effect of free surface proximity, a 100nm sample was also irradiated in-situ with 20keV He+ at 550°C. This produces a uniform low level of He (50x less than ex situ case) implantation, and a gently increasing comparable level of knock-on damage going down through the sample thickness.

Results
The thick "quasi ex situ" samples developed faults on {110} planes at temperatures up to 600°C; at 900°C the fault plane had changed to {111}. Displacement vectors were obtained using g.R analysis; some were found to be from the ½<110> or ½<011> families, some from neither previously observed displacement vector type (Banerjee, Jacobson, Zindell, & Mitchell, 1991). Bubbles of size 1-10nm were found at the He peak in samples irradiated at 480°C and 600°C. At 900°C, large bubbles (>200nm) evolved on grain boundaries and smaller (50-100nm) bubbles in grain interiors at the He peak (Sharp, et al., 2024). The {111} faults were preferentially associated with the grain interior bubbles, implying some kind of free surface or He sink effect at work.
The thin in situ sample contained some faults at room temperature before irradiation, which experienced very little change as the temperature was increased to 550°C. A high density of new faults began to appear almost as soon as He+ irradiation was started. Analysis of prior and irradiation induced faults in the in situ specimen is presented and compared with ex situ work to give an initial step to explaining the relationship between bubbles and faults.

Conclusion

Planar crystal faults are present in unirradiated $TiBe_{12}$; new faults are created on irradiation with high energy (20-300keV) helium ions. At lower temperatures, faults lie on {110} planes, transitioning to {111} planes at some temperature between 600°C and 900°C in constrained material. In the same temperature interval, helium bubbles change from single nm size, to 50-100nm in grain interiors and larger on grain boundaries. Bubbles and {111} faults created at high temperature are preferentially associated.
Next steps in the subject will be to pinpoint the fault transition temperature, and to carry out and simulations and compare with experimental results to find the atomic configurations at {110} and {111} fault types, if there is a volume change between the two types that affects their relationship with bubbles, and whether/how they are sinks for interstitial helium atoms. The same process of understanding must then follow for hydrogen in the structure.

Image caption: ADF-STEM image from sample irradiated ex situ at 900C. White lines are {111} planar faults; small black objects are grain interior bubbles. At bottom is a larger bubble on a grain boundary. Image is part of a montage presented in Sharp et. al. 2024.

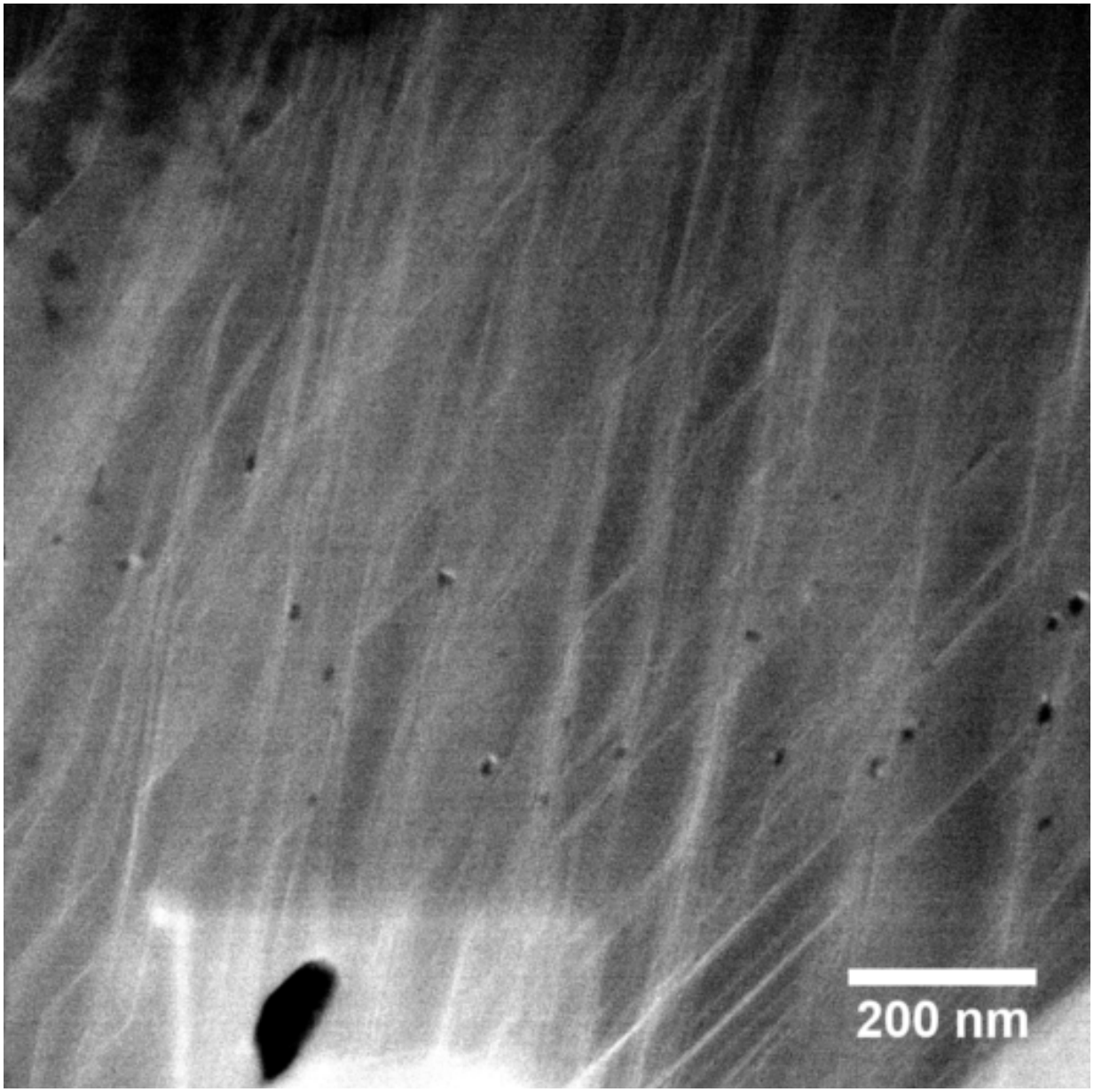

Keywords:

In-situ, irradiation, fusion, beryllide, defects

Reference:

Banerjee, D., Jacobson, L., Zindell, J., & Mitchell, T. E. (1991). The microstructure of titanium beryllide, TiBe12. Materials Research Society Symopsium, 213.
Kim, J.-H., Hwang, T., Nakano, S., Miyamoto, M., Iwakiri, H., & Nakamichi, M. (2021). Deuterium desorption and retention of beryllium intermetallic compounds for fusion applications. Journal of Nuclear Materials, 550, 152936.
Sharp, J., Kuksenko, V., Gaisin, R., Greaves, G., Hinks, J., Vladimirov, P., & Donnelly, S. (2024). Investigation of the microstructure of He+ ion-irradiated TiBe12 and CrBe12 using ex-situ transmission electron microscopy. Journal of Nuclear Materials, 588, 154812. doi:https://doi.org/10.1016/j.jnucmat.2023.154812
Zimber, N., Lammer, J., Vladimirov, P., Kothleitner, G., Keast, V. J., Dürrschnabel, M., & Klimenkov, M. (2023). Hydrogen and helium trapping in hcp beryllium. Communications Chemistry, 6, 76.

1041

Using XeF2 FIB imaging to contrast and quantify precipitation in metal.

Mr Peter Thomas[1], Dr Mariia Zimina[1], Dr Lawrence Coghlan[1], Mr Aidan Gunn[1], Dr Siqi He[1], Dr Aya Shin[2], Dr Jonathan Pearson[2], Professor Peter Flewitt[1], Dr Tomas Martin[1]
[1]University of Bristol, Bristol, United Kingdom, [2]EDF UK, Gloucester, United Kingdom

Poster Group 2

Background incl. aims
Precipitation within a material is known to affect material properties, from mechanical to chemical [1]. Depending on the type, location, orientation, and distribution of precipitates, these properties can vary significantly [2]. In this study we utilize the XeF_2 gas injection system (GIS), a common feature on dualbeam microscopes, in combination with FIB imaging to drastically enhance the contrast of precipitates and therefore make image processing easier. By combining the FIB-XeF_2 technique with low magnification and high resolution, it allows the extraction of large amounts of statistical data using software such as Dragonfly [Computer Software] 2022.2.

Methods
The FIB-XeF_2 contrast mapping procedure and micrograph capture were collected using a ThermoFisher Scios 2 dual-beam FIB system, which contains a gallium ion source. A full procedure can be found in previous work [3]. We have completed this technique using three different materials, all of which had different initial conditions and reasons for evaluating. First, an experimental Fe9Cr1Mo steel exposed to high-temperature and-pressure CO_2 environments, second, a 316H steel that had undergone creep testing, and third, an Alloy 690 nickel-based alloy that has undergone a surface mechanical process.
First, the surface was initially exposed to a high current FIB beam (30kV:50nA) to remove the surface oxide layer and expose hard precipitates in the matrix. The GIS needle was inserted and XeF_2 gas was flowed across the area of interest. Once the GIS needle was retracted, the area of interest was then exposed to a much lower FIB current of 30kV:1nA. Under the influence of this FIB beam, the XeF_2 gas binds preferentially to the metallic matrix and less to the precipitates, resulting in an enhanced contrast effect. This imaging was continued until the maximum contrast between the precipitates and the metal matrix was obtained, following which a high-resolution image was taken. In this study, the final images were taken at a resolution of 6144 x 4096, integrated 4 times with a dwell time of 1 µs. This produced an image of significant quality for quantitative analysis without altering the contrast too much. The precipitates were also individually characterised with Transmission Electron Microscopy (TEM) diffraction, Energy-dispersive X-ray spectroscopy (EDS), and Transmission Kikuchi diffraction (TKD) to identify their crystal structure on elemental composition and diffraction pattern. Once a characteristic of a particular morphology was identified using TEM / EDX / TKD, precipitates of similar contrast and morphology in the FIB-XeF_2 images were labelled as this precipitate identity.

Results
FIB-XeF_2 images were processed using image recognition in Dragonfly [computer software] 2022.2. The features within each image were segmented according to greyscale contrast using an Otsu threshold selection method [4]. This allowed the separation of precipitate from bulk, voids, and subsequently segmented different precipitates into separate virtual objects. The graphic shows an example of this approach – top left shows the raw FIB-XeF_2 image of a region of Fe9Cr1Mo steel, showing a lighter metal matrix and several precipitates with different greyscale contrasts and morphologies. The subsequent subfigures show in pink, blue, and yellow the segmentation of these features into three distinct populations based on greyscale contrast and morphology that were identified using TEM diffraction as $M_{23}C_6$, M_7C_3, and M_2C respectively. These segmented features are

spatially located datasets, that can subsequently be parsed for the following statistical information: area fraction as a function of distance, distribution, size, orientation, and type. This enables quantification of microstructure over large areas with much greater confidence.
For 316H, precipitate locations were combined with grain boundary locations and compared with voids within the sample to obtain directional correlation information across the sample. Complete results for 316H steel can be found in previous work [5].
For the Alloy 690 sample, FIB-XeF_2 images provided clear microstructural information, such as precipitate pocketing along grain boundaries that was missed in other techniques.

Conclusion
Precipitation is an important factor when considering the chemical and mechanical behaviour of a material, especially for a material exposed to extreme environmental conditions. By re-utilising the XeF_2 gas module most dual beam FIB instruments have, it is possible to bring out the contrast of different precipitates against the bulk in such a way that image processing software can easily extract statistical information. This data will lead to a greater understanding of the behaviour of the material.

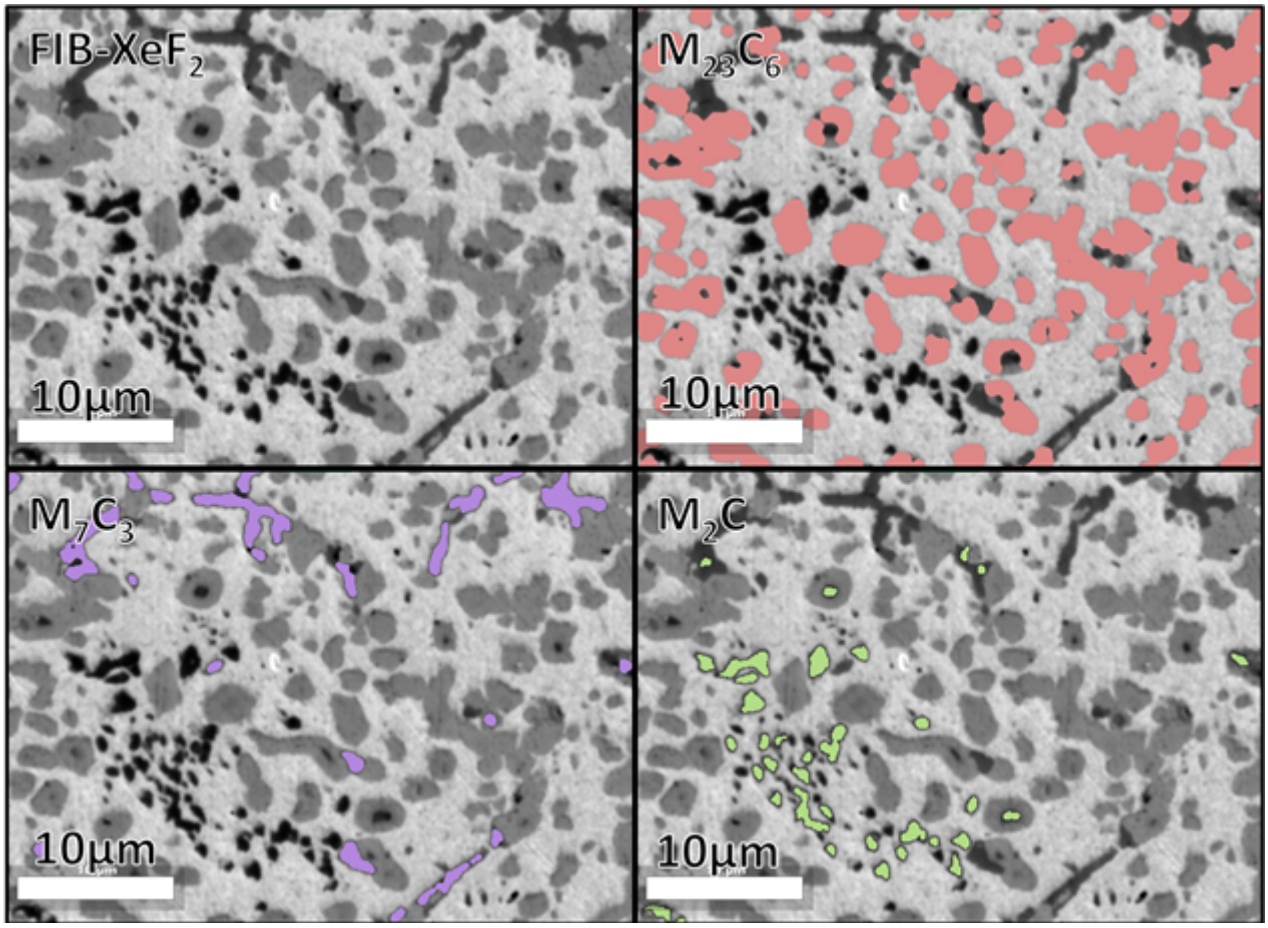

Keywords:

XeF_2, FIB, Contrast, Dragonfly

Reference:

[1] W.D. Callister, D.G. Rethwisch, Materials science and engineering : an introduction, Tenth edition. SI version. Global edition, Wiley Hoboken, NJ, Hoboken, 2020.
[2] L. Coghlan, S. Yan, A. Shin, J. Pearson, M.A.E. Jepson, R.L. Higginson, The effect of microstructure on the oxidation and carburisation of 9Cr-1Mo steel exposed to CO2, Corrosion Science 191, 2021.
[3] P. Thomas, M. Zimina, A. Shin, J. Pearson, P.E.J. Flewitt, T. Martin, Microstructural Evolution due to CO2 Oxidation and Carburisation in Fe9Cr1Mo Steel, in: Transactions of the SMiRT 27, 2024.

[4] N. Otsu, A Threshold Selection Method from Gray-Level Histograms, IEEE Transactions on Systems, Man, and Cybernetics 9,1979.
[5] S. He, E. Horton, S. Moore, E. Galliopoulou, P.J. Thomas, A. Fernandez-Caballero, E. Elmukashfi, M. Salvini, M. Mostafavi, D.M. Knowles, P.E.J. Flewitt, T.L. Martin, A correlative approach to evaluating the links between local microstructural parameters and creep initiated cavities, Materials & Design, 2024.

1073

Influence of damage dose on the defect formation in tungsten

Dipl.-Ing. Ute Jäntsch[1], Dr. Michael Klimenkov[1], Dr. Michael Rieth[1], Dr. Thomas Schwarz-Selinger[2], Dr. Mikhail Zibrov[2]
[1]Institute of Applied Materials, Karlsruhe Institute of Technology, Eggenstein-Leopoldshafen, Germany, [2]Max-Planck-Institut für Plasmaphysik (IPP), Garching, Germany

Poster Group 2

1. Introduction

The development and construction of fusion reactor, such as ITER, have become very important in recent years, as has the development of new construction materials that can withstand the new requirements. Tungsten and tungsten-based alloys are considered as most promising candidate materials for these applications. Due to its favorable thermal and mechanical properties, such as high melting point, high thermal conductivity and low sputtering rate, the alloys were selected as the plasma facing materials in the ITER divertor.
Investigations of their radiation resistance, provide valuable information on the response of components to the fusion plasma. For this propose, tungsten samples were 20 MeV tungsten ion irradiated to create displacement damage and were subsequently loaded with deuterium. The aim of these investigations was to study the cause for the evolution of deuterium retention with damaging dose for samples where the displacement damage was created at a temperature of 1080°C.

2. Materials & methods

Pure W selected for this analysis was annealed at 2000°C so that the grain size increased to ~10 - 50 µm. The W-plates were W-irradiated with 20.3 MeV energy at different damage doses (0.1 dpa, 0.5 dpa and 2.3 dpa) at 1080°C. The thickness of the damaged layer formed in tungsten under these implantation conditions was ~2.5 µm. samples were loaded with deuterium at low energy and low flux (5 eV/D, $5x10^{19}$ D/m^2s) to decorate the existing defects without creating new ones. TEM lamellae preparation was carried out using the electron microscope Crossbeam Auriga, ZEISS. After preparation an electrochemical polishing process (flashing) of the lamellae was performed. The investigations were carried out using transmission electron microscopy (TEM) to determine the existence of voids and their distribution in the matrix over the cross-section, starting from the surface.

3. Results

TEM investigations of the prepared lamellae were performed using bright field imaging for the voids as well as scanning TEM dark field imaging to observe the formation of dislocation loops. The study demonstrates the homogeneous formation of voids in the depth up to 2.5 µm. The voids have a similar average size and a similar density over the whole thickness. The formation of inhomogeneities such as size peaks or number density peaks, which are typical for the implanted layers, was not observed. Figure 1 shows TEM cross-sections along the layers exposed to 0.1 dpa, 0.5 dpa and 2.3 dpa irradiation. The clearly visible fluctuations in the lamellae thickness are caused by the flash polishing of the film. The TEM images of all three tungsten samples clearly show the existence of voids of the nanometer size in the microstructure.

Figure 1: TEM image of the W irradiated to 0.1 dpa, 0.5 dpa and 2.3 dpa with finely distributed voids of different sizes.

4. Conclusions

The microstructure of tungsten irradiated to the damage dose of 0.1 dpa, 0.5 and 2.3 dpa at 1080°C were studied in detail using TEM. In all three samples, the existence of voids could be clearly demonstrated.

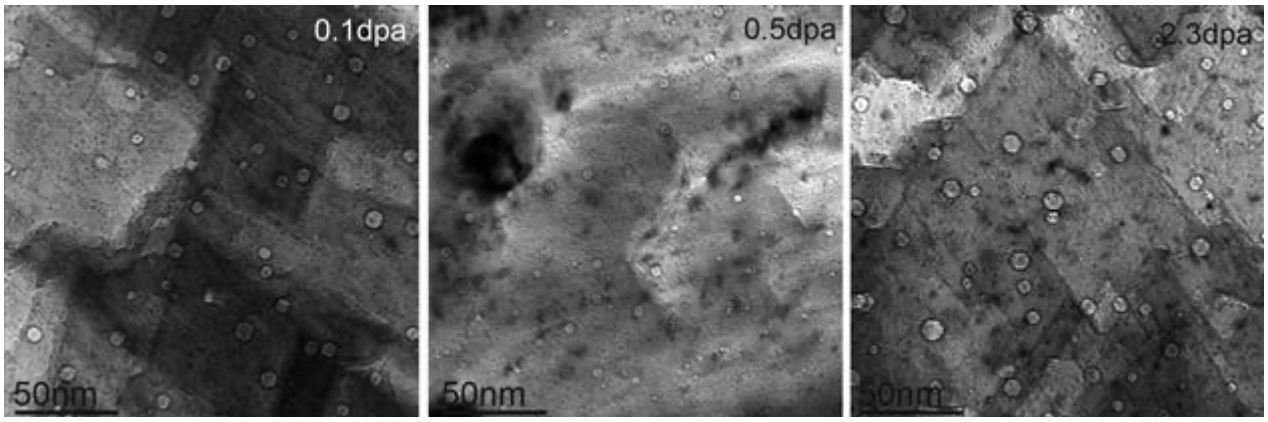

Keywords:

Fusion, Tungsten, FIB, TEM

1077

Corrosion of Alloys Suitable for Very High Temperature Systems (VHTRs) Exposed to High Temperature Helium

Dr Lawrence Coghlan[1], Dr Mariia Zimina[1], Dr Robert Burrows[3], Dr Aya Shin[2], Dr Tomas Martin[1]
[1]University of Bristol, Bristol, United Kingdom, [2]EDF Energy, Gloucester, United Kingdom, [3]National Nuclear Laboratory, Bristol, United Kingdom

Poster Group 2

Background and Aims

During operation of Very High Temperature Reactor (VHTR) systems, the temperatures will be operating at above 700°C where having a high creep strength and corrosion resistance to the high temperature atmosphere is of vital importance [1].

Helium is used within the VHTR systems as the gas is “inert” and helium, in comparison to other potential coolants, does not become radioactive when exposed to neutron radiation. Complications occur due to the presence of carbon (from the graphite in the reactor), any impurities within the helium gas and potential water ingress from the environment[2,3]. These factors, coupled with the very high temperatures of operation, can lead to complex interactions taking place between the helium coolant gas and the metal. These can include oxidation, carburization and decarburization [1,4] and in certain high temperature alloys, for example on Alloy 800 the surface corrosion layer can delaminate which will have a detrimental effect on the physical properties of mechanical components.

These interactions will affect the physical properties of the alloys as the chemistry is altered during exposure to helium at high temperatures and may negatively affect the physical properties of the alloys, for example decarburization will lead to a reduction in carbides which may affect the physical properties of the alloys.

The work here has characterized three high temperature nickel based alloys (Alloy 617, Alloy X and Alloy 800) using advanced microscopy techniques after exposure to high temperature helium (740°C) for various durations with the aim to better understand the interactions taking place within high temperature helium systems.

Methods

Various nickel based alloys have been exposed at 750°C to a helium atmosphere for various durations inside a high temperature tube furnace. These alloys (Alloy 617, Alloy 800 and Alloy X) were selected based on their physical properties and corrosion resistance. Upon removal from the furnace, samples were characterised using advanced microscopy techniques including Scanning Electron Microscopy (SEM) and Focused Ion Beam Microscopy (FIB). These techniques allowed for characterisation of the changes taking place during their exposure to high temperature helium. Elemental Dispersive X-Ray Spectroscopy (EDS) was used to characterise the elements within the corrosion layer and to highlight the elemental changes which take place at these high temperatures.

Results

Analysis of the samples shows differences in the oxidation/corrosion behaviour of the different alloys dependant on exposure duration. A comparison between three alloys exposed at 750°C to helium for 1000 hours is shown in the Figure where different morphologies can be seen across the surface of the alloys. The corrosion layer thickness and morphology varied for the different materials with precipitates and oxide nodes developing near to the surface of the exposed surface.

Conclusion

The corrosion behaviour of alloys exposed to high temperature helium is of importance to understand for use within VHTR systems. The work here has characterised three alloys and shown the differences in the oxidation characteristics for each alloy. This will help to better understand corrosion process taking place within a high temperature environment when exposed to helium.

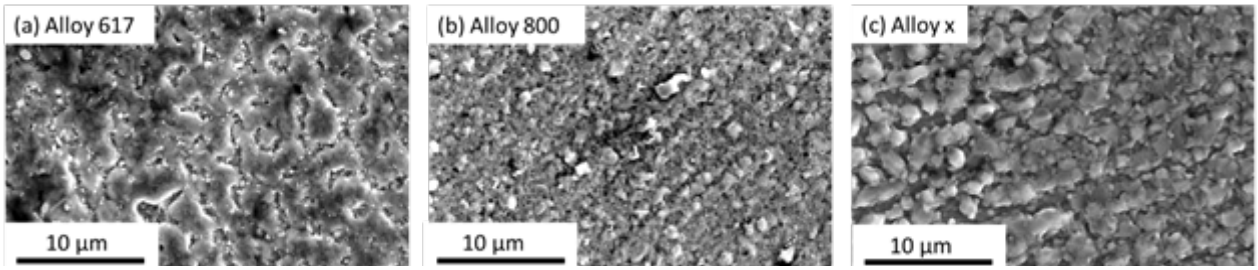

Keywords:

Oxidation, High Temperature Corrosion, Microscopy

Reference:

[1] C. Cabet, A. Terlain, P. Lett, L. Guétaz, J.M. Gentzbittel, High temperature corrosion of structural materials under gas-cooled reactor helium, Materials and Corrosion 57 (2006) 147–153. https://doi.org/10.1002/maco.200503901.

[2] W. Zheng, B. Du, H. Li, H. Yin, X. He, T. Ma, High temperature corrosion of two superalloys in the impure helium environment, J Nucl Sci Technol 60 (2023) 923–929. https://doi.org/10.1080/00223131.2022.2159893.

[3] J. Berka, M. Vilémová, P. Sajdl, Testing of degradation of alloy 800 H in impure helium at 760 °C, Journal of Nuclear Materials 464 (2015) 221–229. https://doi.org/10.1016/j.jnucmat.2015.03.054.

[4] H. Li, W. Zheng, B. Du, H. Yin, X. He, T. Ma, X. Yang, The high temperature corrosion of Incoloy 800H alloy at three different atmospheres, J Nucl Sci Technol 60 (2023) 165–174. https://doi.org/10.1080/00223131.2022.2089756.

1267

Fatigue fracture behaviour of high strength steels under gaseous hydrogen

Dr Elina Saarivirta Huttunen[1], Pekka Pohjanne[1], Dr Pekka Moilanen[1], Dr Jouni Alhainan, Dr Supriya Nandy[1]
[1]VTT Technical Research Center of Finland Ltd, , Finland

Poster Group 1

Structural steels suffer from hydrogen embrittlement (HE) at various stages of its value chain. Versatility of steel microstructures necessitates detailed investigation about how HE occurs at various microstructural hierarchies and interfaces. In this study, we examine the role of various boundaries in two key steel microstructures, i.e., direct quench martensitic steel (DQ1600) - consisting >99% martensite, and quench-partitioned martensitic steel (QP1900) - consisting up to 10% retained austenite and 90% martensite.
We used in-house built bellow-devised fatigue testing set up, to examine fatigue behaviour in pressurized hydrogen atmosphere. Fatigue tests of these microstructures were carried out using 100 bar gaseous H2 (pre-charged + in-situ charging) using 0.03 Hz frequency, under ambient condition using 86 Hz frequency, using stress ratio of -1 under variety of stress amplitudes. Tests were carried out until fracture and fracture surfaces of the selected specimens were investigated using scanning electron microscope. Selected fracture surfaces were cut across the cross-section along the primary crack propagation direction. After standard metallographic polishing, we examined the cross-sections using electron backscatter diffraction (EBSD).
We observed up to 3 orders of deterioration in fatigue life under the influence of 100 bar H2 environment compared to ambient atmosphere in both the steel microstructure. Effect of these microstructures on the fracture events, during HE, is widely different. In ambient conditions as well in pressurized N2, both steels demonstrate similar fracture behaviour, depicted by occurrence of fatigue striations. In hydrogen, on the other hand, DQ1600 steel shows prevalent plasticity mediated intergrannular (IG) fracture, whereas, QP1900 steel exhibits dominant quasi-cleavage (QS) transgrannular (TG) fracture event. Image analyses from the cross-section of the selected samples indicate that depth of secondary cracks (SCs) at 1 mm from the initiation point is twice in case of DQ1600 steel compared to QP1900 one. EBSD-assisted analyses in determining the contribution of various boundaries towards SCs propagation suggests that compared to ambient condition, in case of HE, SCs activated along different lath interfaces in both steels. Using Kurdjumov-Sachs relationship, we showed that in case of DQ1600 steel subjected to HE, block boundaries dominated the fracture events; whereas, in case of QP1900 steel, the sub-block boundaries and lath interface fracture were more prevalent.
In conclusion, local plasticity mediated decohesion, also known as hydrogen induced local plasticity (HELP) mediate hydrogen enhanced decohesion embrittlement (HEDE) is observed to be more dominant in DQ1600 steel compared to QP1900 steel, in which decohesion is more prevailing at microstructural hierarchs.

Keywords:

hydrogen embrittlement, EBSD, fatigue, interface

Reference:

Nagao, A., Dadfarnia, M., Somerday, B. P., Sofronis, P., & Ritchie, R. O. (2018). Hydrogen-enhanced-plasticity mediated decohesion for hydrogen-induced intergranular and “quasi-cleavage” fracture of lath martensitic steels. Journal of the Mechanics and Physics of Solids, 112, 403-430.
Morito, S., Tanaka, H., Konishi, R., Furuhara, T., & Maki, A. T. (2003). The morphology and crystallography of lath martensite in Fe-C alloys. Acta materialia, 51(6), 1789-1799.